Improved potentiometric SECM imaging of galvanic corrosion reactions

D. Filotás[1,2], B. M. Fernández-Pérez[3], J. Izquierdo[3,4], A. Kiss[1], L. Nagy[1,2], G. Nagy[1,2], R. M. Souto[3,4]

[1] Department of General and Physical Chemistry, Faculty of Sciences, University of Pécs, Ifjúság útja 6, 7624 Pécs, Hungary.

[2] János Szentágothai Research Center, University of Pécs, Ifjúság útja 20, 7624 Pécs, Hungary.

[3] Department of Chemistry, Universidad de La Laguna, P.O. Box 456, E-38200 La Laguna, Tenerife, Canary Islands, Spain.

[4] Institute of Material Science and Nanotechnology, Universidad de La Laguna, E-38200 La Laguna, Tenerife, Canary Islands, Spain.

Abstract

The galvanic corrosion of Zn-Cu systems has been monitored in situ using scanning electrochemical microscopy in the potentiometric mode. Here, the initial studies performed using double-barrel microelectrodes for the simultaneous detection of local pH and Zn ion concentration changes in single lines scans, have been extended to the obtention of 2-D maps of Cu^{2+} and Zn^{2+} ions. The construction and calibration of a novel Cu^{2+} ion selective microelectrode is reported. New scanning algorithms and data evaluation tools have been explored for faster acquisition rates than those limited by the time constants associated to potentiometric response.

Keywords: Copper; Zinc; Scanning electrochemical microscopy; Ion selective microelectrode; Galvanic corrosion; Local pH distribution.

1. Introduction

The Scanning Electrochemical Microscope (SECM) has become an essential tool for the local characterization of the mostly heterogeneous processes occurring on corroding metal surfaces exposed to aqueous environments [1-4]. In general, amperometric microelectrodes are the usual sensing probes in Scanning Electrochemical Microscopy (SECM) studies [5], and the same occurs in corrosion studies [1-4]. However, since the selectivity of an amperometric probe is poor, because the recorded current response at the tip may result from the redox conversion of more than one chemical species, the SECM operation with ion selective microelectrodes (ISME) is advantageous in a number of real applications [6-8]. The main limitation for their widespread use is the slower time constants associated to the potentiometric response [9], although the performance of these devices is rapidly improving thanks to the development of solid contact ion-selective microelectrodes (ISME) of smaller internal resistance and faster response times [10,11].

In order to monitor complex processes, multi-channel electrodes are efficient devices, yet to date this type of electrodes have been employed mainly in life sciences. Multi-barrel micropipettes were developed in the early eighties to monitor different ion levels simultaneously in clinical research, and they are employed in iontophoresis [12-16]. In some cases, they are effectively single ion selective electrodes whereas the other barrels are employed to deliver chemicals [17]. These devices are built placing the electrode in the inner core surrounded by the other capillaries. Alternately, McCarthy et al. employed titanium-based multi-channel electrodes for recording neural signals [18], whereas Piironen et al. developed carbon microtetrodes for neuroanalytical applications [19]. The neurons vary in size and morphology, thus this electrode with multiple recording sites was a powerful tool for the detection of extracellular voltage signals. On the other hand, Walker et al. fabricated and applied triple-barrel electrodes, including a reference electrode, to measure K^+ ions and pH in barley root cells [20].

One example of corrosion process with a mechanism involving multiple redox reactions occurs while galvanically coupling dissimilar metals or metal phases, resulting in the formation of local microanodes and microcathodes in the micrometer scale on the surfaces of the materials exposed to the aqueous environment [21-25]. Along with the actual redox processes involved in the oxidation/reduction processes occurring in each microcell [26-28], pH changes related to both the cathodic process and the hydrolysis of

dissolved metals strongly influence the corrosion rate [29-32]. The simultaneous occurrence of pH distributions and heterogeneous zinc ion release from model galvanic pairs has been imaged using scanning electrochemical microscopy operated in potentiometric mode [33-36] or the scanning ion electrode technique (SIET) [37-39]. In these studies, the concentration distributions of each species were actually imaged in separate single experiments as it was necessary to exchange the ion-selective measuring probe involved. Though quite good correlations have been attained from those separated measurements [33-39], the simultaneous monitoring of pH and zinc ion distributions in galvanic corrosion processes is desirable. Yet, due to the rather slow scanning rates required for imaging with ISME probes, the investigation of the dynamic corrosion reactions with high spatial resolution has been mostly based on the measurement of single scan lines instead [33-36], and recording of the actual 2D distribution maps could be scarcely attempted [40].

An interesting approach towards multi-signal acquisition has been performed by Lamaka and coworkers using multi-head stages for either separate ion-selective microelectrodes [41], or the combination of a single ISME with a SVET probe [41-43]. Although measurements were performed along one single scan, the rather big distance required between the two probes hindered simultaneous acquisition of two signals at the same point, actually imposing a certain delay between them. In some way, the operation of such multi-head configuration resembled actual separate measurements with each probe, although avoiding the replacement of the probe in actual single probe experiments. An alternative route has been recently reported by our groups for chemical imaging by SECM using ion-selective microelectrodes. It consisted of a double barrel microelectrode probe that contained a Zn-ion selective and a pH-sensitive Sb-based microelectrodes sharing a common scanning tip. In this way, simultaneous recording of Zn-ion and pH concentration distributions were obtained for the first time, although the very slow scan rates imposed by the time constants of the microelectrodes prevented actual recording of 2D maps and the time evolution of a dynamic corrosion process had to be established from single line scans [40]. Simultaneously, new scanning algorithms and data evaluation methods allowing faster acquisition rates have been developed [45-47], and although they have only been tested for model current sources using noble metals, it is considered that it opens new possibilities for the in situ study of corrosion processes using potentiometric SECM.

In this work, the operation of a double-barrel sensor for the simultaneous detection of Zn^{2+} and pH in SECM investigation of corrosion reactions using a Zn-Cu galvanic pair exposed to aqueous chloride solution has been extended to the obtention of 2D maps by the application of scanning algorithms and data evaluation methods that allow faster recording rates. In addition, we report the fabrication, calibration and operation of a new solid contact Cu^{2+} selective microelectrode and its combination with Zn ISME in the double-barrel arrangement for the imaging of model Zn-Cu galvanic corrosion processes as well as their selectivity for the simultaneous monitoring of Cu^{2+} and Zn^{2+} ions due to their potential applicability for the monitoring of brass dezincification. The improvement of potentiometric SECM operation for the spatially-resolved characterization of corrosion processes is demonstrated from selected experiments.

2. Experimental

2.1. Double-barrel capillary probes

Micropipettes were fabricated from borosilicate capillaries (outer diameter Ø = 1.5 mm, inner dia. Ø = 1.0 mm, obtained from Hilgenberg GmbH, Malsfeld, Germany). Double-barrel capillary probes were prepared by attaching together two capillaries using a copper wire for fixation. The two capillaries were heated and twisted by 180° using a Narishige PE-2 puller (Tokyo, Japan). After cooling, the resulting double-barrel capillaries were pulled in another heating process to obtain the desired final micrometer dimensions. The obtained double-barrel capillary was soaked in “piranha” solution and thoroughly washed with ultrapure water (Millipore water system, specific conductivity $\kappa = 5.6\times10^{-8}$ S cm^{-1}; Merck Millipore, Billerica, MS, USA). Silanization of the capillaries was accomplished by soaking in 5% vol. solution of dichloro-dimethyl-silane in CCl_4 (Sigma Aldrich, MO, USA), and then kept in oven at 120 °C for 30 min.

The Zn-ion selective microelectrode was prepared by adapting the solid contact method developed for the fabrication of the Mg^{2+}-ISME in ref. [48]. A carbon fiber of 33 μm diameter (obtained as a generous gift from Specialty Materials, Lowell, MA, USA) was introduced inside one of the capillaries of the double-barrel assembly. It was employed to ensure the internal contact with the ionophore cocktail, whereas the other

end of the fiber was glued to a copper wire with silver epoxy adhesive (Epofix, Struers, Ballerup, Denmark) to provide an electrical connection to the external equipment. The portion of the carbon fiber to be inserted in the cocktail was coated by electrochemical polymerization of 3,4-ethylenedioxythiophene (EDOT, HC Starck GmbH, Goslar, Germany)) dissolved in 1-butyl-3-methylimidazolium hexafluorophosphate ($BMIM^+$ PF_6^-) ionic liquid [49]. The electrochemical cell used for electropolymerization was composed by the carbon fiber as working electrode, a chlorinated Ag wire as reference electrode, and a Pt wire as the auxiliary electrode. The ionophore cocktail for the Zn ISME's was produced using Zinc ionophore I (1 mg), tetrahydrofurane (THF, 98 μL), 2-nitrophenyl octyl ether (oNPOE, 42 μL), poly(vinyl chloride) (PVC, 2.04 mg), and potassium tetrakis(4-chlorophenyl)borate (PTCB, 0.22 mg). The Cu^{2+} selective microelectrodes were prepared using copper (II) ionophore IV (1 mg), oNPOE (0.22 mg), PVC (2.26 mg), and THF (98 μL). All the membrane components were supplied by Sigma Aldrich (St. Louis, MO, USA). A small amount of the ion selective coating was allocated into the micropipette tip with a syringe under suction, followed by inserting the PEDOT coated carbon fiber. Finally, Loctite® adhesive was used to seal the rear of the ISME.

A homemade antimony microelectrode was used to measure local pH. A few grams of antimony powder were melted above the roaring flame of a Bunsen burner, and a single barrel capillary was filled with a small volume of the molten metal using a 50 mL syringe, while applying vacuum at the opposite end of the capillary. The intact sections of the glass sealed antimony wire were submitted to several pulling steps to obtain fibers in the appropriate disc diameter range. 1.5-2.0 cm long antimony fibers were introduced and positioned at the orifice of the remaining capillary of the double barrel assembly. The electric contact between the abraded copper wire and the antimony fiber was attained using liquid mercury. The diameter of the antimony fibers ranged 15-30 μm.

Figure 1 shows optical micrographs of the finished double-barrel probe. The responses of the Zn-ISME and pH sensors in the double barrel arrangement were characterized and satisfactorily compared with the behavior of single-barrel probes, as reported in the literature. Calibration of the Zn-ISME was accomplished using a set of solutions of controlled Zn^{2+} ion activities. It showed linear behavior with slope -28.5 mV $decade^{-1}$ in the $1 \leq pZn \leq 5$ range (where $pZn = -\log a_{Zn^{2+}}$). Analogously, there was

linearity for the Sb-based microelectrode in the interval $4 \leq pH \leq 10$, with -50.5 mV decade^{-1} slope. Similar sub-Nernstian responses have been previously reported for Sb-based microelectrodes based on polycrystalline antimony [8,34-36].

2.2. SECM instrumentation

Potentiometric SECM experiments were performed using a homemade instrument. Custom software was designed to allow the use of the new scanning patterns and high scan rate. High input impedance ($Z_{in} = 10^{13}$ Ω) voltage meters (eDAQ isopod, Denistone East, NSW, Australia) were used to measure the potential difference between the reference and the measuring electrodes. The reference electrode was a home-made miniature Ag/AgCl/(3.5 M) KCl electrode (E^0 = +0.197 V vs. NHE). To minimize wiring capacitance, a short (ca. 20 cm length) coaxial wire was used for the electrical connection between the electrodes and the instrument. Specific scan parameters are indicated in the figure captions. The sample was placed at the bottom of the electrochemical cell, whereas the local potential values of the double-barrel microelectrodes were measured with respect to the same reference electrode. Deconvolution of the SECM images was performed as described in [47].

2.3. Samples and test solutions

The Zn-Cu galvanic pair consisted of iron and copper wires of 200 µm diameter. They were embedded into Epofix resin sleeve (Struers, Ballerup, Denmark) with 1 mm separation between them. Another set of samples was produced using single wires of Cu (2 mm diameter) and Fe (1 mm diameter), embedded into Epofix resin sleeve. Surface finish of the top side of the metal samples was done by wet grinding with emery papers of 800-4000 grit size, followed by polishing with Micropolish II alumina slurries (Buehler, Lake Bluff, IL, USA) in 96 vol.% ethanol down to 0.3 µm particle size. The samples were rinsed with acetone and Milli-Q water, and dried in air. The sample was surrounded laterally by Sellotape creating a cylindrical container for approximately 3.5 mL of the test solution, thus exposing the circular cross sections of the two metals upwards. Electrical contact between the two metals was performed at the rear of the sample.

Model Zn^{2+} and Cu^{2+} ion sources were made using micropipettes inserted in a plastic container. Two holes were drilled about 1 cm far from each other and two micropipettes of about 100 μm diameter orifice were allocated upside down through the holes. The pipettes were previously filled with 5% agar-agar gel saturated with either copper sulfate or zinc sulfate.

For calibration and SECM experiments, $CuSO_4 \cdot 5H_2O$, $ZnSO_4 \cdot 7H_2O$, NaCl, and KCl were obtained from Reanal (Budapest, Hungary). Test solutions were prepared using the corresponding analytical grade chemical and ultrapure Milli-Q water without addition of a supporting electrolyte. Experiments were conducted at ambient temperature in the naturally-aerated solutions.

3. Results and discussion

Potentiometric operation of the SECM can be particularly advantageous for chemical imaging in corrosion studies as the potentiometric probes have superior selectivity over amperometric probes. However, this can be also a drawback, because one can monitor only one species at a time, and corrosion processes frequently involve several simultaneously ongoing reactions with the participation of various different species. The concentration changes of these species bear important information about the corrosion process. Simultaneous detection of different species can be a major contribution to the understanding of mechanisms in Corrosion Science. On the other hand, conventional ion selective microelectrodes have relatively long response times; hence, a compromise between scanning time and resolution and image quality is usually required. An additional limitation may arise from insufficient selectivity of the ISME employed in corrosion research. The anodic and cathodic reactions produce different chemical species and it is necessary to establish if the ISME employed selectively measures the activity of the ion of interest. This issue can be of special relevance in the investigation of alloys, due to the competitive dissolution reactions of different metals. In this paper, we describe two experimental methods employed to enhance the performance of ion selective microelectrodes in SECM experiments by allowing faster scan acquisition rates. Next, the design and operation of a Cu-ISME is described. Finally, the simultaneous monitoring of local Zn^{2+} and Cu^{2+} activities using double-

barrel electrodes is extended to characterize their superior performance in the galvanic corrosion of Zn-Cu systems, while assuring adequate selectivity for these ions.

3.1. Galvanic corrosion of a model Zn-Cu pair

The Zn-Cu galvanic pair immersed in 1 mM NaCl solution was considered to be an adequate corrosion system for testing the suitability of the double-barrel probe assembly in potentiometric SECM operation, as it allows the simultaneous visualization of concentration profiles and distribution of several species involved in a highly dynamic corrosion process. Experiments were always performed with the two metals electrically connected at the rear of the sample, thus effectively originating a galvanic pair of controlled geometry. The strong driving force yields significant anodic dissolution from the zinc disc. In this arrangement, the anodic reaction, namely metal dissolution, occurs on the less noble metal as given by:

$$Zn \rightarrow Zn^{2+} + 2e^{-} \quad (1)$$

Furthermore, the dissolved metal ions may undergo hydrolysis, a process that is greatly affected by the pH of the environment as to originate either zinc-containing hydroxo complex ions (eqns. (2), (4) and (5)) or insoluble $Zn(OH)_2$ (eqn. (3)) [50,51]:

$$Zn^{2+} + H_2O \rightarrow Zn(OH)^{+} + H^{+} \quad (2)$$

$$Zn(OH)^{+} + H_2O \rightarrow Zn(OH)_2 + H^{+} \quad (3)$$

$$Zn(OH)_2 + H_2O \rightarrow Zn(OH)_3^{-} + H^{+} \quad (4)$$

$$Zn(OH)_3^{-} + H_2O \rightarrow Zn(OH)_4^{2-} + H^{+} \quad (5)$$

Therefore, local acidification would be the result of zinc hydrolysis reactions. In a naturally-corroding environment, and most especially in the case of a very thin electrolyte layer as it occurs in the case of atmospheric corrosion, it is unlikely that hydrolysis of electrically-insulated zinc would lead to the formation of other species than $Zn(OH)^{+}$ due to the accumulation of H^{+} from the first stage of the hydrolysis reaction, a process generally defined as zinc run off [52]. Under those conditions, precipitation of corrosion products is usually the result of combined dry-humid periods. Conversely, subsequent hydrolysis stages can occur in the case of galvanic corrosion reactions under continuous immersion in a naturally aerated electrolyte solution, due to the combined effect of a greater bulk electrolyte volume and the driven force of the more noble metal for the consumption of the electrons released by zinc during its corrosion. This is precisely the case with the sample and cell geometries adopted in this

model experiment, and therefore the extent of the zinc hydrolysis reactions will be mostly determined by the pH of the electrolyte. Furthermore, the 1 mm separation between the two metal wires in the sample was regarded sufficient to prevent precipitation of corrosion products on the active surface of the metals. In the rare event that precipitation might occur within the short time scale of the experiments described here, precipitation would occur over the resin as the separation distance should be sufficient to maintain both half-cell reactions separated.

On the other hand, the electrons released by zinc in the electric circuit connecting the two metals are taken by dissolved oxygen to be reduced on the copper surface according to:

$$O_2 + 2H_2O + 4e^- \rightarrow 4OH^- \quad (6)$$

Therefore, the cathodic half-cell reaction contributes to alkalization of the electrolytic environment.

Potentiometric SECM imaging of the model Zn-Cu galvanic pair immersed in NaCl aqueous solution was performed by translating the dual microelectrode probe relative to the sample placed horizontally at the bottom of the small electrochemical cell. Figure 2A shows a pH map recorded above the connected Zn-Cu pair in 1 mM NaCl. Local alkalization above the copper cathode and acidification above the zinc anode are readily observable, although the quality of the recorded image is very poor. It is known that the distortion of the image in potentiometric SECM is the consequence of the relatively long response time of the probe. If the probe moves between two points, where the theoretical difference $E_{\text{cell}(0)}$-$E_{\text{cell}(\infty)}$ is the potential measured at the previous point of the scan, but the acquisition time is not sufficient for the potentiometric cell to reach the steady potential signal at the current point, the measured potential (i.e., $E_{\text{cell}(t)}$) at the acquisition time t will be:

$$E_{\text{cell}(t)} = E_{\text{cell}(\infty)} + \left[E_{\text{cell}(0)} - E_{\text{cell}(\infty)}\right] e^{-\frac{t}{RC}} \quad (7)$$

where R is mainly the resistance of the microelectrode, and C is the sum of the input capacitances of the amplifier in the voltage follower and of the wires connecting the amplifier and the electrodes. Thus, the resulting image will be distorted. Deconvolution of the raw data can significantly improve the quality of the image [46,47]. In brief,

rearrangement of eqn. (7) shows that the potential could be determined in the case of infinitely long equilibration time by knowing the time constant of the ISME used as sensing probe, and measuring the potential at *t* equilibrating time. In this way, more reliable images can be obtained even in the case of blurred images recorded at high scanning rate. Figure 2B shows the pH distribution over the Zn-Cu galvanic couple resulting from the application of the deconvolution procedure to the raw image given in Figure 2A.

Another approach consists in the use of scanning algorithms optimized for the sample geometry. Since samples of circular shape are imaged in SECM practice quite frequently, a scanning pattern optimized for circularly symmetric samples was described in [45]. Indeed, comb-like distortion can be observed in published works using potentiometric SECM imaging. This issue is even more significant when considering the image given in Figure 2A. This pH map was recorded using the frequently-employed meander mode for acquisition, where the probe scanned a rectangular area by executing a series of line scans (see Figure 3A). In brief, the scanning direction along the *X* axis alternated from line to line, so as the probe reached the last raster point of the line, for instance in the *X*+ direction, and when the measurement for that certain point was finished, it moved one step in the *Y* direction and continued the scan in the opposite direction (*X*-). The red circle in Figure 3A indicates the starting point, the green dots are the measurements points, and the blue circle is the last point of the raster procedure. Using the meander algorithm for scanning, a characteristic distortion can show up, associated to the change in scan direction between consecutive lines.

In this work, the applicability of the scanning algorithm proposed in ref. [45], combined with the deconvolution analysis technique introduced in reference [43], was investigated in a real dynamic corrosion reaction such as Zn-Cu galvanic pair immersed in 1 mM NaCl aqueous solution. The goal was to make possible the use of higher scan rates for potentiometric SECM imaging. In the case of circularly symmetric targets as the metal disks employed in this work, the use of circular scanning algorithms becomes an attractive possibility. Therefore, the polar scan algorithm described in Figure 3B was next employed, that is initiated at the centre of the metal samples and progresses outwards along a spiral trajectory. A typical measurement is shown in Figure 3D. It must be noticed that the images are displayed in squares, though the measurement itself

holds circular symmetry as shown in Figure 3C. The typical square presentation is obtained by extrapolating the largest measurement circle to estimate the values for the edges of the square (cf. Figure 3D). The white + signs in the 2D maps of Figure 3C-D, depict the actual measurement points.

The superior resolution of the concentration distributions obtained using the experimental procedure described in this work is evidenced by direct inspection of Figure 4. The images B, D and F show the pH and Zn ion distributions simultaneously recorded over the Zn and Cu wires using the dual microelectrode probe of Figure 1. For the sake of comparison, the same images obtained using the conventional meander mode are also given. Therefore, acquisition of 2D images of a dynamic corrosion system by potentiometric SECM both resolved spatially and in time has been shown to be feasible by adopting new scanning algorithms and deconvolution procedures for the recorded data. Importantly, potentiometric SECM can perform in situ simultaneous monitoring of various chemical species relevant to the corrosion process using double barrel probes containing specific ISME as to distinguish surface domains with similar topography and morphology but different electrochemical properties, while assessing the localized corrosion rates for each domain. In this way, there is no need to run separate experiments or to perform probe exchange for monitoring various signals of interest, and dynamic processes in corrosion research can be resolved by the acquisition and comprehensive quantitative analysis (with deconvolution) of data obtained in a single area scan. Since different combinations of pH and zinc concentration values can greatly influence the extent of metal hydrolysis processes in the electrolyte, spatially resolved concentration profiles should contribute to a better understanding of the actual corrosion processes involved in the distributed microcells dynamically developing on the metal surfaces.

3.2. Development of a Cu ISME

In the previous section, potentiometric SECM operation was performed on an ideal galvanic pair system, because the anodic and cathodic reactions were spatially separated over the two metal wires, and zinc dissolution was the only reaction expected in the anode. In many cases however, simultaneous dissolution of different species takes place on the surface of the investigated sample. Then the selectivity of the ISME is of paramount importance to establish the reliability of the measurements. Any released

interfering ion would affect the measured potential, and by using a conventional single-barrel ISME arrangement one cannot ascertain the extent of such interference and obtain the actual distributions of the primary and interfering ions. In this context, the use of multi-barrel electrodes becomes greatly advantageous. In this work, the simultaneous detection of zinc (II) and copper (II) ions using the double-barrel electrode arrangement was investigated. To this end, a solid contact Cu^{2+} ISME was constructed and subsequently characterized.

The calibration of the Cu^{2+} selective electrode in the double barrel assembly was performed using 10^{-6} to 10^{-1} M $CuSO_4$ solutions without the addition of any supporting electrolyte. The procedure was initiated with the most diluted solution, followed by solutions of increased concentration. The calibration curve exhibited an almost Nernstian response (27.2 mV decade^{-1}) in the 10^{-1} to 10^{-5} M range, with 1.05×10^{-5} M as the lowest detection limit (see Figure 5). The same calibration methodology was employed for the Zn ISME in the double barrel assembly. A Nernstian slope (28.5 mV decade^{-1}) was found in a wide concentration range, and the lowest limit of detection was 9.33×10^{-6} M. The selectivities of these ISME to the other primary ion were also determined using the separate solution method [27]. The corresponding logarithmic selectivity coefficients for the Cu ISME and the Zn ISME were log $K_{Cu,Zn}$ = -3.91, and log $K_{Zn,Cu}$ = -0.78, respectively.

Next, the internal resistance of the ionselective microelectrodes was measured using the voltage divider method [53]. Resistors with sufficiently high resistivity were selected to this end (i.e., R_k = 100-150 MΩ). The potential of the cell was measured against the Ag/AgCl/(3.5 M) KCl reference electrode using a high input impedance voltmeter. After attaining steady open circuit potential, U_{OCP}, the resistor R_k was switched in the circuit and the resulting voltage (U_k) was measured. The resistance of the ISME electrode was then determined from the potential difference ΔU (i.e., $\Delta U = U_{OCP} - U_k$) using the following equation [53]:

$$R_{\mathrm{ISME}} = \frac{\Delta U \cdot R_k}{U_k} \qquad (8)$$

It is generally accepted that more precise values can be determined when U_k is close to $½U_{OCP}$ [53]. Therefore, the resistance value was obtained by averaging 3 $\Delta U/U_k$ values, and it was found to be 373 MΩ.

Two model experiments were performed to test the applicability of the new Cu ISME for SECM experiments. The Cu^{2+} ISME was first used to image the dissolution of copper from a polarized pure copper sample immersed in 0.1 M KCl. Prior to the actual measurement, copper was subjected to galvanostatic activation by applying a constant current density of 1 mA cm^{-2} during 1 min. Immediately after the polarization was stopped, the Cu-ISME was positioned over the center of the metal strip at 50 μm height, and a potentiometric map was recorded following a polar scan pattern starting from the centre of the sample. Figure 6A depicts the approximately three orders of magnitude concentration change occurring in the close vicinity of the polarized copper disc as result of the previous polarization step. It must be noticed that the potentiostat was switched off while recording the scan.

In the second experiment, an iron disc (2 mm diameter) was employed as Cu^{2+} sink while immersed in 10^{-2} M $CuSO_4$ solution. Due to the different galvanic potential of the two metals, Cu^{2+} ions are reduced over the surface of the Fe sample, and the concentration of this species becomes locally depleted compared to the bulk solution. Therefore, it was expected that the translation of the Cu-ISME over the iron wire would monitor a potential decrease. Indeed, after positioning the Cu-ISME over the iron disc specimen at 50 μm height, 3 mL of 10^{-2} M $CuSO_4$ solution was introduced in the small electrochemical cell containing the iron disc at its bottom, and after 10 s of waiting time, significant decreases of the local Cu^{2+} concentrations were observed above the metal (cf. Figure 6B). The results obtained in these two model experiments imply that the Cu ISME can be employed for the potentiometric SECM characterization of corrosion reactions in real systems.

3.3. Simultaneous operation of double barrel Cu and Zn ISME probes

The selectivity of the Cu and Zn ion selective microelectrodes in a double barrel assembly was investigated using copper(II) and zinc(II) ion point sources. To this end, micropipettes were filled with 5% agar-agar gel saturated with the sulfate salt of the ion of interest. The scheme of the experimental system is given in Figure 7A, whereas Figure 7B shows the double barrel assembly containing the Zn and Cu ISME. This probe was scanned above the two metal ion point sources, and the signals of the Zn ISME and Cu ISME were recorded simultaneously. Figure 8 shows the corresponding

concentration distributions of Cu^{2+} and Zn^{2+} ions recorded over each micropipette ion source. As it was expected, about half order of magnitude increase of the Cu^{2+} concentration was measured above the Cu^{2+} ion source using the Cu ISME in Figure 7A. Analogously, the Zn^{2+} map recorded above the other micropipette shows higher values, close to 1 order of magnitude increase. On the other hand, the Zn^{2+} source caused only 1-1.5 mV change in the signal measured by the Cu ISME, due to the good selectivity of the Cu ISME (cf. Figure 8C). Unfortunately, the selectivity of the Zn ISME is poorer for Cu^{2+} ions as it was shown in the previous section. As result, an apparent Zn^{2+} concentration peak was recorded above the pipette containing $CuSO_4$ in Figure 8D, that is clearly an artifact. These findings require further consideration in relation to the potential applicability of this double barrel ISME probe to more complex systems such as brass dezincification. Since the Cu ISME is not completely selective for copper, the potential change caused by zinc dissolution will contribute to the potential signal recorded by the Cu ISME. Concomitantly, zinc dissolution will be also overestimated using the Zn ISME due to the interfering effect of copper dissolution. Therefore, a new analytical procedure has been derived using the advantageous combination of two ISME in the double barrel assembly. Although both electrode potentials will be biased by the analyte ion of the other, they can be expressed using the Nicolsky-Eisenman equation [54] as follows:

$$E_{\mathrm{Zn}} = E_{0,\mathrm{Zn}} + S_{\mathrm{Zn}}\log(a_{\mathrm{Zn}} + K_{\mathrm{Zn,Cu}}a_{\mathrm{Cu}}) \quad (9)$$

$$E_{\mathrm{Cu}} = E_{0,\mathrm{Cu}} + S_{\mathrm{Cu}}\log(a_{\mathrm{Cu}} + K_{\mathrm{Cu,Zn}}a_{\mathrm{Zn}}) \quad (10)$$

where E_{Zn} and E_{Cu} are the measured potential at each ISME; $E_{0,\mathrm{Zn}}$ and $E_{0,\mathrm{Cu}}$ are the potentials measured at unity activity of the subscripted ions (namely 1 M), and they include all the constant potential contributions measured; S_{Zn} and S_{Cu} are the slopes of the Zn^{2+} and Cu^{2+} ISME calibration plots; a_{Zn} and a_{Cu} are the activities of the Zn^{2+} and Cu^{2+} ions; $K_{\mathrm{Zn,Cu}}$ and $K_{\mathrm{Cu,Zn}}$ are the selectivity coefficients of the Zn^{2+} and Cu^{2+} ISME, respectively. All the variables in these two equations are known with the exception the ion activities. Therefore, there are two equations with two unknowns, and the logarithmic activity of the zinc(II) ions can be written as:

$$a_{\mathrm{Zn}} = 10^{[(E_{\mathrm{Zn}} - E_{0,\mathrm{Zn}})/S_{\mathrm{Zn}}]} - K_{\mathrm{Zn,Cu}} a_{\mathrm{Cu}} \quad (11)$$

whereas the Cu(II) activity can be expressed as:

$$a_{\mathrm{Cu}} = \frac{10^{[(E_{\mathrm{Cu}} - E_{0,\mathrm{Cu}})/S_{\mathrm{Cu}}]} - K_{\mathrm{Cu,Zn}} \cdot 10^{[(E_{\mathrm{Zn}} - E_{0,\mathrm{Zn}})/S_{\mathrm{Zn}}]}}{1 - K_{\mathrm{Cu,Zn}} \cdot K_{\mathrm{Zn,Cu}}} \quad (12)$$

This evaluation method was employed to correct the artifact observed in Figure 8D. The measured and the calculated Zn(II) concentration distributions above the Cu(II) ion source scan are given in Figure 9. It can be seen that the apparent Zn(II) concentration originally recorded over the center of the Cu-source has been completely removed by using this analytical procedure, attaining potential values similar to those in the bulk of the electrolyte away from the ion sources. Although some apparent Zn(II) ion distribution is still found at the edges of the sample, it must be noticed that the 0.25 orders of magnitude change in Zn(II) activity recorded in the original map decreased to 0.13 after data processing. The reason for the remaining apparent Zn distribution is due to pattern differences in the simultaneously recorded pZn and pCu images. The “ring” around the sample seems to be an error in the measurement. This implies that the analytical method proposed is not operating at 100% confidence level, although it performs excellently in the center of the sample where the biggest change in Cu(II) concentration occurred, and thus the biggest interference in the Zn(II) measurement is expected.

4. Conclusions

Although a fraction of a second is enough for the acquisition of an image in STM or in AFM with spatial resolution in the micrometer range, the long time needed for SECM measurements, particularly when a high resistance potentiometric tip is used, remains a problem. This is especially relevant when chemical information is gathered about a dynamic process such as corrosion reactions. In this context, it has been shown

here that imaging of concentration distributions in galvanic corrosion processes with high spatial resolution can be achieved by potentiometric SECM using double barrel ISME assemblies. The experimental approach described here was based on the combination of a new scanning algorithm based on the symmetry of the sample and the application of deconvolution analysis for faster acquisition. As result, images were recorded at significantly higher scan rates than those limited by the time response of the ion selective microelectrodes employed as probes.

The applicability of the method for a dynamic corrosion reaction has been first shown for the simultaneous measurement of pH and zinc ion distributions from a spontaneously corroding Zn-Cu galvanic pair immersed in naturally aerated 1 mM NaCl solution at ambient temperature. Next, the proposed methodology has been extended to the simultaneous monitoring of Zn and Cu ion distributions using model ion point sources. It is proposed that the experimental and evaluation methodology described in this paper has the potential to be employed for the monitoring of more complex corrosion reactions such as the brass dezincification process.

In addition to simultaneous measurement, the combination of two or more ion selective microelectrodes in a multi barrel assembly allows sufficient selectivity of the ISME to be resolved by establishing an equation set containing the same number of unknowns and equations.

Acknowledgements

The work was financially supported by the Spanish Ministry of Economy and Competitiveness (MINECO, Madrid) and the European Regional Development Fund under grant CTQ2016-80522-P, the National Research, Development and Innovation Office (Budapest, Hungary) under grant K125244, and the “Environmental industry related innovative trans- and interdisciplinary research team development in the University of Pécs knowledge base under SROP-4.2.2.D-15/1/Konv-2015-0015 project. D.F. thanks the Erasmus Mobility programme for a mobility grant to University of La Laguna.

References

1. S.E. Pust, W. Maier, G. Wittstock, Investigation of localized catalytic and electrocatalytic processes and corrosion reactions with scanning electrochemical microscopy (SECM), Z. Phys. Chem. 222 (2008) 1463–1517.
2. L. Niu, Y. Yin, W. Guo, M. Lu, R. Qin, S. Chen, Application of scanning electrochemical microscope in the study of corrosion of metals, J. Mater. Sci. 44 (2009) 4511–4521.
3. R.M. Souto, S.V. Lamaka, S. González, Uses of scanning electrochemical microscopy in corrosion research, in: A. Méndez-Vilas, J. Díaz (Eds.), Microscopy: Science, Technology, Applications and Education, Vol. 3, Formatex Research Center, Badajoz (Spain), 2010, pp. 1769-1780.
4. M.B. Jensen, D.E. Tallman, Application of SECM to corrosion studies, in: A.J. Bard, C. Zoski (Eds.), Electroanalytical Chemistry: A Series of Advances, Vol. 24, CRC Press, Boca Raton (FL, USA), 2012, pp. 171-286.
5. A.J. Bard, M.V. Mirkin (Eds.), Scanning Electrochemical Microscopy, 2nd edition. CRC Press, Boca Raton (FL, USA), 2012.
6. K. Hu, Y. Gao, Y. Wang, Y. Yu, X. Zhao, S.A. Rotenberg, E. Gökmese, M.V. Mirkin, G. Friedman, Y. Gogotsi, Platinized carbon nanoelectrodes as potentiometric and amperometric SECM probes, J. Solid State Electrochem. 17 (2013) 2971-2977.
7. M. Serrapede, G. Denuault, M. Sosna, G. L. Pesce, R.J. Ball, Scanning electrochemical microscopy: Using the potentiometric mode of SECM to study the mixed potential arising from two independent redox processes, Anal. Chem. 85 (2013) 8341–8346.
8. J. Izquierdo, L. Nagy, I. Bitter, R.M. Souto, G. Nagy, Potentiometric scanning electrochemical microscopy for the local characterization of the electrochemical behaviour of magnesium-based materials, Electrochim. Acta 87 (2013) 283-293.
9. E. Lindner, Y. Umezawa, Performance evaluation criteria for preparation and measurement of macro- and microfabricated ion-selective electrodes (IUPAC Technical Report), Pure Appl. Chem. 80 (2008) 85-104.
10. R. Zhu, Z. Ding, Enhancing image quality of scanning electrochemical microscopy by improved probe fabrication and displacement, Can. J. Chem. 83 (2005) 1779-1790.

11. G. Gyetvai, S. Sundblom, L. Nagy, A. Ivaska, G. Nagy, Solid contact micropipette ion selective electrode for potentiometric SECM, Electroanalysis 19 (2007) 1116-1122.
12. M. Fujimoto, M. Honda, Direct measurement of intracellular Na and K activities in the renal tubular cells with triple-barreled micro-electrodes, in: L. Takács (Ed.). Kidney and Body Fluids, Akadémiai Kiadóo, Budapest, 1981, pp. 341-350.
13. M. Chesler, pH regulation in the vertebrate central nervous system: microelectrode studies in the brain stem of the lamprey, Can. J. Physiol. Pharmacol. 65 (1985) 986-993.
14. M.B.A. Djamgoz, J. Dawson**,** Procedures for manufacturing double-barrelled ion-sensitive microelectrodes employing liquid sensors, J. Biochem. Biophys. Methods 13 (1986) 9-21.
15. P.W. Dierkes, S. Neumann, G. Klees, W.-R. Schlue, Multi-barrelled ion-selective microelectrodes as tools for the investigation of volume regulation mechanisms in invertebrate nerve cells under hyperosmotic conditions, Electrochim. Acta 48 (2003) 3373-3380.
16. J.S.T. Deveau, M.I. Lindinger, B. Grodzinski, An improved method for constructing and selectively silanizing double-barreled, neutral liquid-carrier, ion-selective microelectrodes, Biol. Proced. Online 7 (2005) 31-40
17. E. Ujec, E.E.O. Keller, N.K.V. Pavlík, J. Machek, Low-impedance, coaxial, ion-selective, double-barrel microelectrodes and their use in biological measurements, Bioelectrochem. Bioenergetics 7 (1980) 363-369.
18. P.T. McCarthy, R. Madangopal, K.J. Otto, M.P. Rao, Titanium-based multi-channel, micro-electrode array for recording neural signals, Conf. Proc. IEEE Eng. Med. Biol. Soc. 5 (2009) 2062-2065.
19. A. Piironen, M. Weckström, M. Vähäsöyrinki, Ultrasmall and customizable multichannel electrodes for extracellular recordings, J. Neurophysiol. 105 (2011) 1416–1421.
20. D.J. Walker, S.J. Smith, A.J. Miller, Simultaneous measurement of intracellular pH and K^+ or NO_3^- in barley root cells using triplebarreled, ion-selective micro electrodes, Plant Physiol. 108 (1995) 743-751.
21. H.S. Isaacs, The measurement of the galvanic corrosion of soldered copper using the scanning vibrating electrode technique, Corros. Sci. 28 (1988) 547-558.

22. A.J. Aldykiewicz Jr., H.S. Isaacs, Dissolution characteristics of duplex stainless steels in acidic environments, Corros. Sci. 40 (1998) 1627-1646.
23. A.C. Bastos, A.M. Simões, M.G. Ferreira, Corrosion of electrogalvanized steel in 0.1 M NaCl studied by SVET, Port. Electrochim. Acta 21 (2003) 371-387.
24. R.M. Souto, Y. González-García, A.C. Bastos, A.M. Simões, Investigating corrosion processes in the micrometric range: A SVET study of the galvanic corrosion of zinc coupled with iron, Corros. Sci. 49 (2007) 4568-4580.
25. K.B. Deshpande, Experimental investigation of galvanic corrosion: Comparison between SVET and immersion techniques, Corros. Sci. 52 (2010) 2819–2826.
26. E. Tada, S. Satoh, H. Kaneko, The spatial distribution of Zn^{2+} during galvanic corrosion of a Zn/steel couple, Electrochim. Acta 49 (2004) 2279-2285.
27. A.C. Bastos, M.G. Taryba, O.V. Karavai, M.L. Zheludkevich, S.V. Lamaka, M.G.S. Ferreira, Micropotentiometric mapping of local distributions of Zn^{2+} relevant to corrosion studies, Electrochem. Commun. 12 (2010) 394–397.
28. J. Izquierdo, L. Nagy, S. González, J.J. Santana, G. Nagy, R.M. Souto, Resolution of the apparent experimental discrepancies observed between SVET and SECM for the characterization of galvanic corrosion reactions, Electrochem. Commun. 27 (2013) 50-53.
29. E. Tada, K. Sugawara, H. Kaneko, Distribution of pH during galvanic corrosion of Zn/steel surface, Electrochim. Acta 49 (2004) 1019-1026.
30. K. Ogle, S. Morel, D. Jacquet, Observation of self-healing functions on the cut edge of galvanized steel using SVET and pH microscopy, J. Electrochem. Soc. 153 (2006) B1-B5.
31. T.N. Vu, P. Volovitch, K. Ogle, The effect of pH on the selective dissolution of Zn and Al from Zn-Al coatings on steel, Corros. Sci. 67 (2013) 42-49.
32. E.A. Zdrachek, A.G. Karotkaya, V.A. Nazarov, K.A. Andronchyk, L.S. Stanishevskii, V.V. Egorova, M.G. Taryba, D. Snihirova, M. Kopylovich, S.V. Lamaka, H^{+}-selective microelectrodes with optimized measuring range for corrosion studies, Sens. Actuator B-Chem. 207 (2015) 967–975.
33. J. Izquierdo, L. Nagy, Á. Varga, I. Bitter, G. Nagy, R.M. Souto, Scanning electrochemical microscopy for the investigation of corrosion processes: measurement of Zn^{2+} spatial distribution with ion selective microelectrodes, Electrochim. Acta 59 (2012) 398-403.

34. J. Izquierdo, L. Nagy, Á. Varga, J.J. Santana, G. Nagy, R.M. Souto, Spatially resolved measurement of electrochemical activity and pH distributions in corrosion processes by scanning electrochemical microscopy using antimony microelectrode tips, Electrochim. Acta 56 (2011) 8846-8850.
35. B.M. Fernández-Pérez, J. Izquierdo, S. González, R.M. Souto, Scanning electrochemical microscopy studies for the characterization of localized corrosion reactions at cut edges of coil-coated steel, J. Solid State Electrochem. 18 (2014) 2983-2992.
36. B.M. Fernández-Pérez, J. Izquierdo, J.J. Santana, S. González, R.M. Souto, Scanning electrochemical microscopy studies for the characterization of localized corrosion reactions at cut edges of painted galvanized steel as a function of solution pH, Int. J. Electrochem. Sci. 10 (2015) 10145-10156.
37. S.V. Lamaka, O.V. Karavai, A.C. Bastos, M.L. Zheludkevich, M.G.S. Ferreira, Monitoring local spatial distribution of Mg^{2+}, pH and ionic currents, Electrochem. Commun. 10 (2008) 259-262.
38. A. Alvarez-Pampliega, S.V. Lamaka, M.G. Taryba, M. Madani, J. De Strycker, E. Tourwé, M.G.S. Ferreira, H. Terryn, Cut-edge corrosion study on painted aluminum rich metallic coated steel by scanning vibrating electrode and micro-potentiometric techniques, Electrochim. Acta 61 (2012) 107–117.
39. A. Alvarez-Pampliega, M.G. Taryba, K. Van den Bergh, J. De Strycker, S.V. Lamaka, H. Terryn, Study of local Na^+ and Cl^-distributions during the cut-edge corrosion of aluminum rich metal-coated steel by scanning vibrating electrode and micro-potentiometric techniques, Electrochim. Acta 102 (2013) 319–327.
40. D. Filotás, B.M. Fernández-Pérez, J. Izquierdo, L. Nagy, G. Nagy, R.M. Souto, Novel dual microelectrode probe for the simultaneous visualization of local Zn^{2+} and pH distributions in galvanic corrosion processes, Corros. Sci. 114 (2017) 37-44.
41. M.G. Taryba, M.F. Montemor, S.V. Lamaka, Quasi-simultaneous mapping of local current density, pH and dissolved O_2, Electroanalysis 27 (2015) 2725–2730.
42. S.V. Lamaka, M. Taryba, M.F. Montemor, H.S. Isaacs, M.G.S. Ferreira, Quasi-simultaneous measurements of ionic currents by vibrating probe and pH distribution by ion-selective microelectrode, Electrochem. Commun. 13 (2011) 20-23.
43. M. Taryba, S.V. Lamaka, D. Snihirova, M.G.S. Ferreira, M.F. Montemor, W.K. Wijting, S. Toews, G. Grundmeier, The combined use of scanning vibrating

electrode technique and micro-potentiometry to assess the self-repair processes in defects on "smart" coatings applied to galvanized steel, Electrochim. Acta 56 (2011) 4475-4488.

44. M.G.Taryba, K.Van den Bergh, J.De Strycker, O.Dolgikh, J.Deconinck, S.V.Lamaka, Novel use of a micro-optode in overcoming the negative influence of the amperometric micro-probe on localized corrosion measurements, Corros. Sci. 95 (2015) 1-5.
45. A. Kiss, G. Nagy, New SECM scanning algorithms for improved potentiometric imaging of circularly symmetric targets, Electrochim. Acta 119 (2014) 169-174.
46. A. Kiss, G. Nagy, Deconvolution of potentiometric SECM, Electroanalysis 27 (2015) 587-590.
47. A. Kiss, G. Nagy, Deconvolution of potentiometric SECM images recorded with high scan rate, Electrochim. Acta 163 (2015) 303-309.
48. J. Izquierdo, A. Kiss, J.J. Santana, L. Nagy, I. Bitter, H.S. Isaacs, G. Nagy, R.M. Souto, Development of Mg^{2+} ion-selective microelectrodes for potentiometric scanning electrochemical microscopy monitoring of galvanic corrosion processes, J. Electrochem. Soc. 160 (2013) C451-C459.
49. S. Bodor, J.M. Zook, E. Lindner, K. Tóth, R.E. Gyurcsányi, Electrochemical methods for the determination of the diffusion coefficient of ionophores and ionophore–ion complexes in plasticized PVC membranes, Analyst 133 (2008) 635–642.
50. S. Thomas, N. Birbilis, M.S. Venkatraman, I.S. Cole, Corrosion of zinc as a function of pH, Corrosion 68 (2012) 65-73.
51. S. Thomas, I.S. Cole, M. Sridhar, N. Birbilis, Revisiting zinc passivation in alkaline solutions, Electrochim. Acta 97 (2013) 192– 201.
52. E. Mena, R.M. Souto, L. Veleva, Early stages of zinc corrosion and runoff process induced by Caribbean sea water, Int. J. Electrochem. Sci. 10 (2015) 7596-7605.
53. S.V. Lamaka, M.G. Taryba, M.L. Zheludkevich, M.G.S. Ferreira, Novel solid-contact ion-selective microelectrodes for localized potentiometric measurements, Electroanalysis 21 (2009) 2447-2453.
54. R.-I. Stefan, J.F. van Steden, H.Y. Aboul-Enein, Electrochemical Sensors in Bioanalysis, Marcel Dekker, New York, 2001.

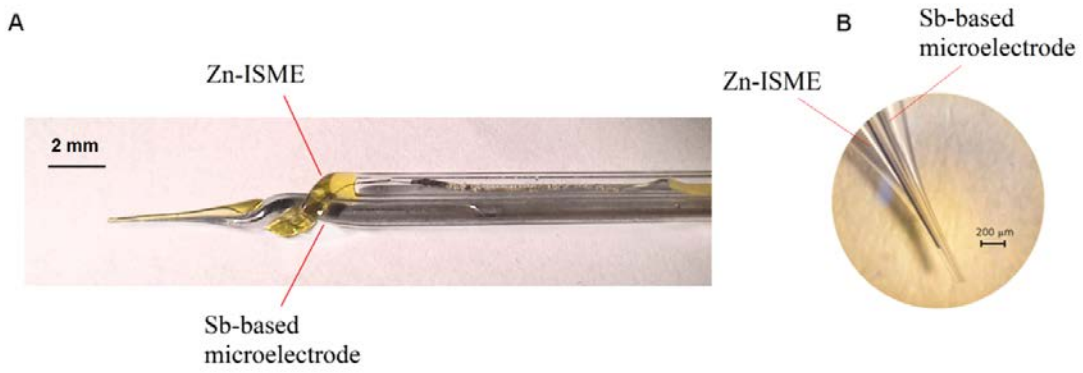

Figure 1. Optical micrographs of the double-barrel microelectrode employed for the simultaneous detection of pH and zinc ion distributions using potentiometric SECM.

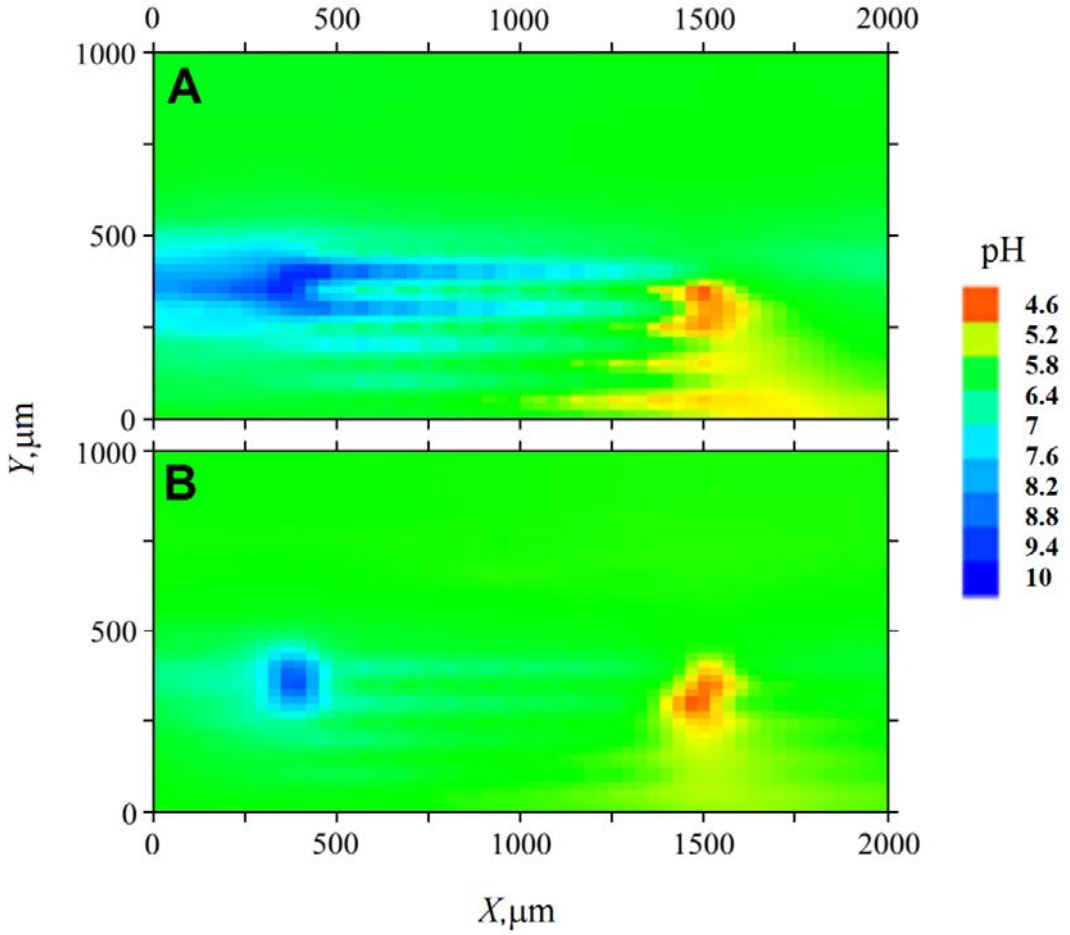

Figure 2. pH distribution above the copper-zinc galvanic couple immersed in 1 mM NaCl. (A) Original, and (B) deconvoluted images. Probe-substrate distance: 50 µm; scan rate: 50 µm s^{-1}. The image was acquired in the meander mode.

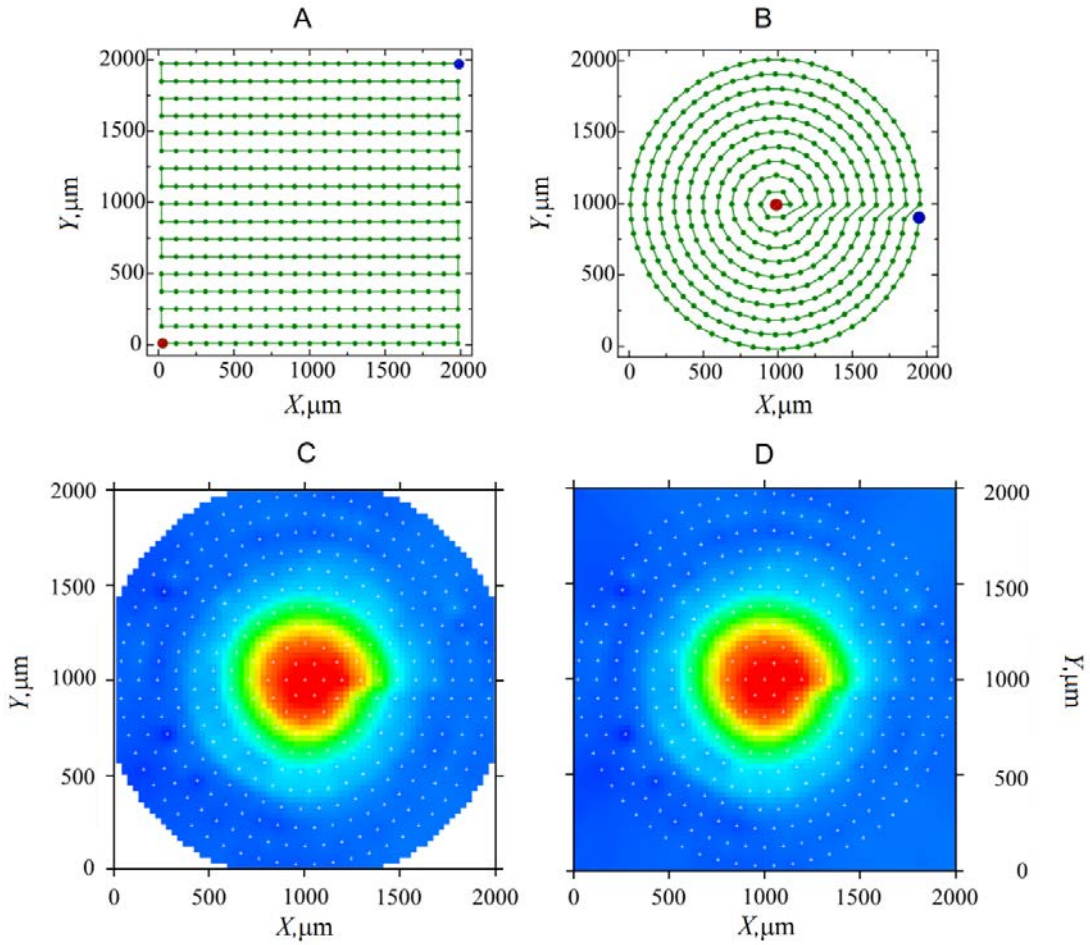

Figure 3. (A,B) Sketches of the two algorithms employed for recording the 2D potentiometric SECM images in this work: (A) meander and, (B) polar algorithms. The blue dots indicate the starting points, red dots are the measurement points, and the green dot is the last point of the scan. (C,D) Zinc concentration distributions recorded above the zinc sample of a Zn-Cu galvanic couple immersed in 1 mM NaCl. (C) Actual measurement using the polar algorithm, and (D) after extrapolation of the largest measurement circle to estimate the values for the edges of the square. Probe-substrate distance: 50 µm; scan rate: 50 µm s^{-1}.

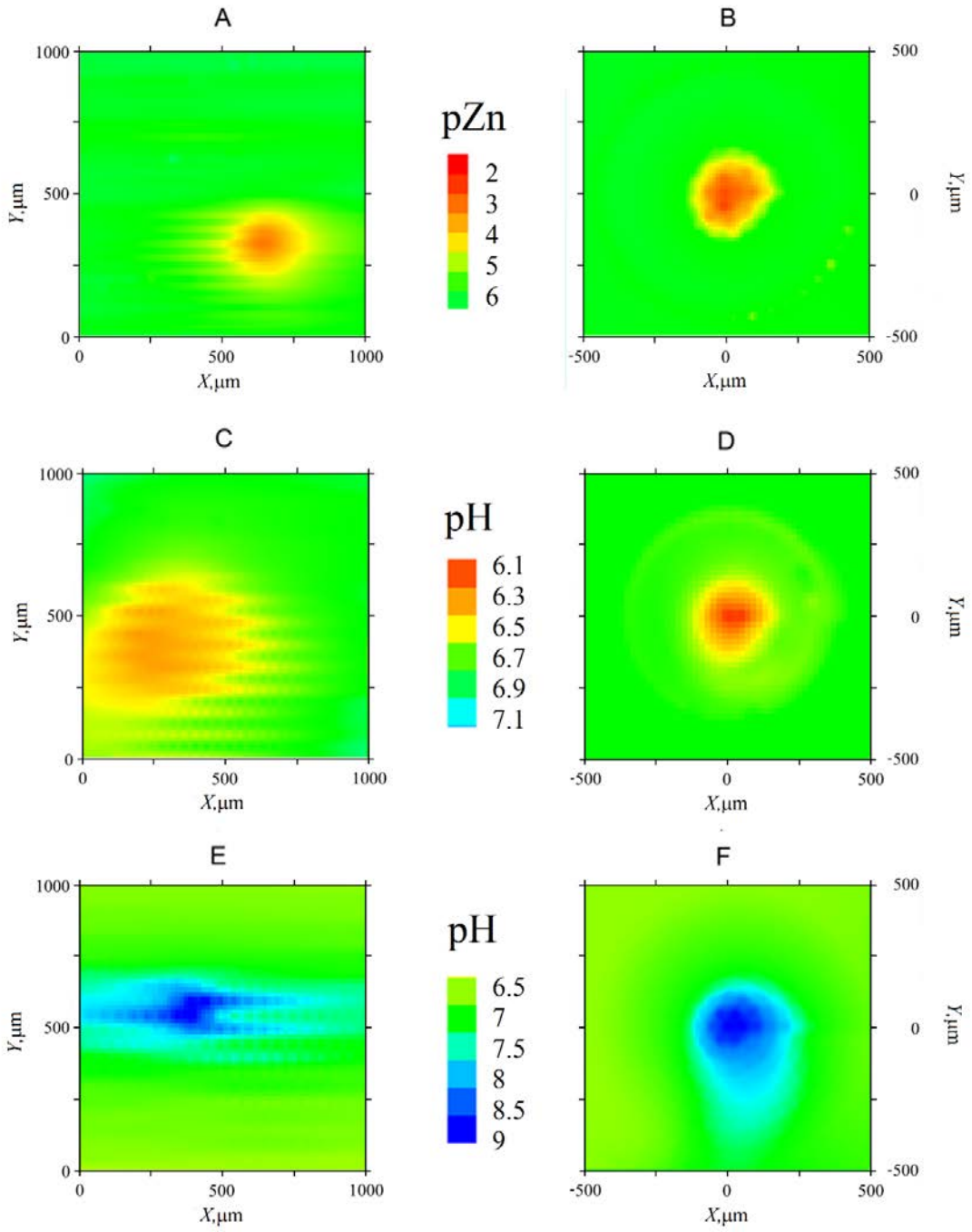

Figure 4. Potentiometric 2D scans obtained over the zinc-copper galvanic couple immersed in 1 mM NaCl using the double barrel assembly for the simultaneous detection of pH and zinc ion distributions. Images were acquired using: (A,C,E) conventional meander, and (B,D,F) polar algorithms. (A,B) zinc ion distribution above the zinc sample; (C,D) pH distribution above the zinc sample; (E,F) pH distribution above the copper sample. Probe-substrate distance: 50 µm; scan rate: 50 µm s^{-1}.

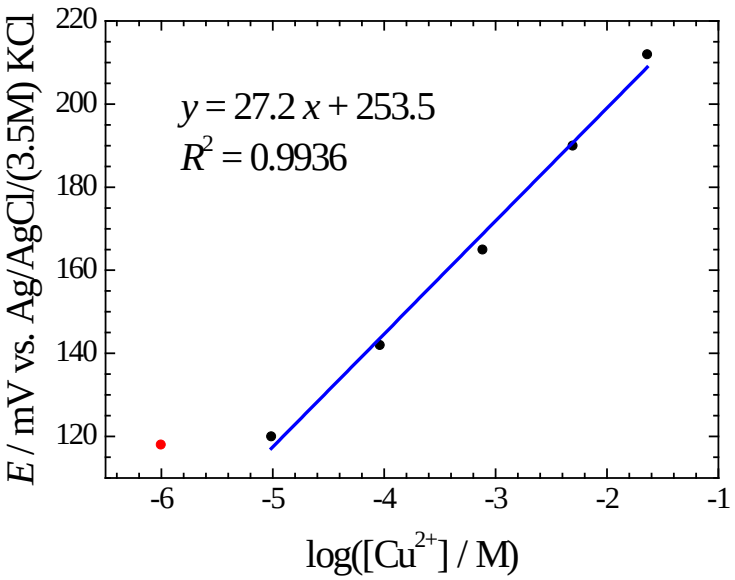

Figure 5. Calibration plot of the potentiometric response of the Cu^{2+} ion selective microelectrode in aqueous solutions containing only different concentrations of $CuSO_4$. Measurements were performed at 22 °C.

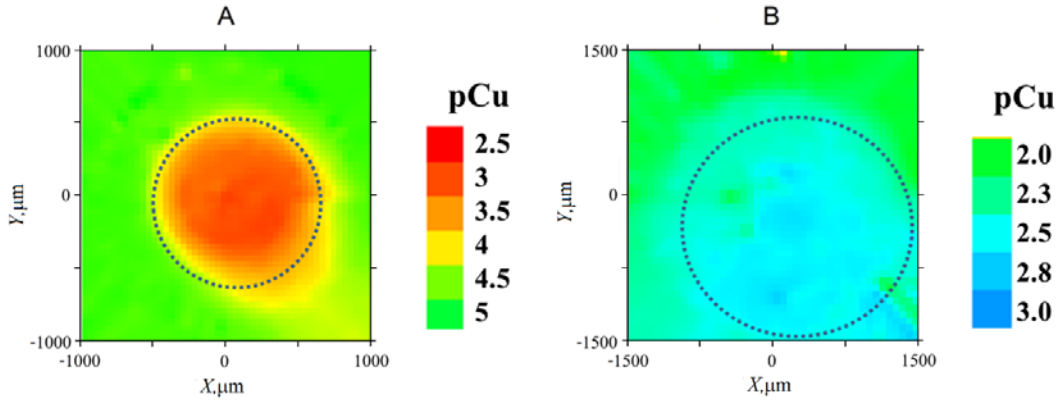

Figure 6. Potentiometric SECM experiments using the new Cu(II) ion-selective microelectrode. A: Cu(II) concentration distribution above a copper wire immersed in 0.1 M KCl immediately after completing 10 min anodic polarization at 0.5 V vs. Ag/AgCl/(3.5 M) KCl. (B) Cu(II) concentration distribution above a Fe wire immersed in 0.01 M $CuSO_4$ solution. Spontaneous deposition of copper occurred over the iron wire resulting in the local depletion of Cu(II) concentration.

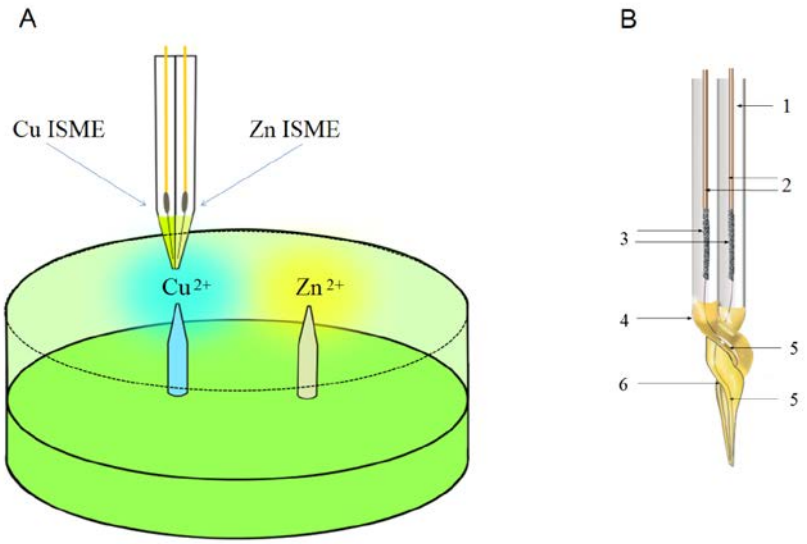

Figure 7. Sketches of (A) assembly for Cu and Zn ion point sources, and (B) Zn/Cu ISME double barrel assembly: 1: double-barrel borosilicate capillary, 2: copper wires, 3: Ag-epoxy, 4: Cu^{2+} ion selective cocktail, 5: PEDOT coated carbon fiber (∅=30µm), 6: Zn^{2+} ion-selective cocktail.

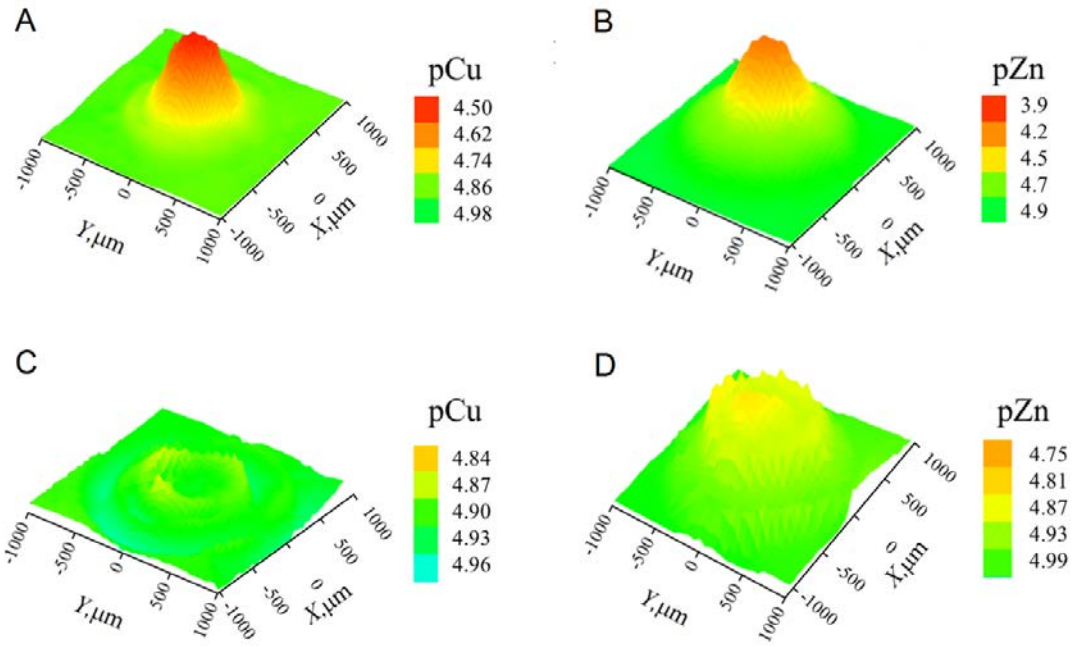

Figure 8. Simultaneous measurements above Cu^{2+} and Zn^{2+} ion sources obtained using the Zn/Cu ISME double barrel assembly: (A) Cu ISME response above the Cu^{2+} ion source; (B) Zn ISME response above the Zn^{2+} ion source; (C) Zn ISME response above the Cu^{2+} ion source; (D) Zn ISME response Zn^{2+} ion source.

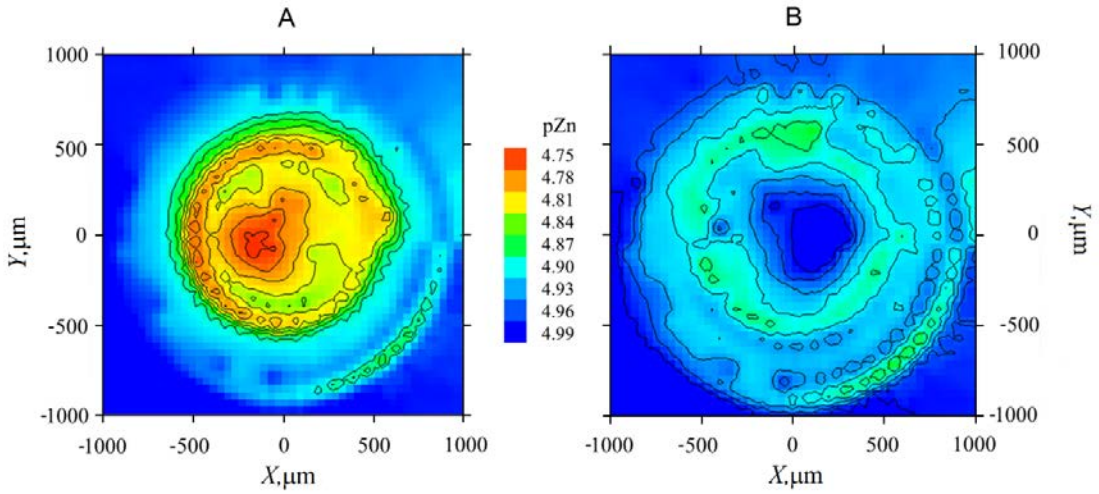

Figure 9. (A) Raw pZn map measured above the Cu^{2+} ion source with the Zn ISME in the double barrel assembly; (B) calculated pZn map using the pCu data simultaneously obtained with the double-barrel assembly.